Numerical simulations of dense suspensions rheology using a DEM-Fluid coupled model

D.Marzougui, B.Chareyre
Laboratoire Sols, Solides, Structures, Grenoble, France
donia.marzougui@3sr-grenoble.fr, bruno.chareyre@3sr-grenoble.fr
and
J.Chauchat
Cemagref de Grenoble - Unité ETNA, Saint Martin d'Hères, France
julien.chauchat@grenoble-inp.fr

ABSTRACT

The understanding of dense suspensions rheology is of great practical interest for both industrial and geophysical applications and has led to a large amount of publications over the past decades. This problem is especially difficult as it is a two-phase media in which particle-particle interactions as well as fluid-particle interactions are significant. In this contribution, the plane shear flow of a dense fluid-grain mixture is studied using the DEM-PFV coupled model. We further improve the original model: including the deviatoric part of the stress tensor on the basis of the lubrication theory, and extending the solver to periodic boundary conditions. Simulations of a granular media saturated by an incompressible fluid and subjected to a plane shear at imposed vertical stress are presented. The shear stress is decomposed in different contributions which can be examined separately: contact forces, lubrication forces and drag forces associated to the poromechanical couplings.

INTRODUCTION

The rheology of grain-fluid mixtures is subject of practical interest for both industrial and geophysical applications. When the solid fraction of such mixture is high enough, *i.e.* in dense suspensions, the bulk behavior is affected by intricated phenomena combining the viscosity of the fluid phase as well as the interactions between the solid particles through solid contacts. Moreover, the contact interactions may be modified by the presence of the fluid, as described by lubrication theories. Additionally, in transient situations, poromechanical couplings may develop long range interactions by coupling the local rate of volume change to the pore

pressure field. Direct particle-scale modeling of this problem is a promising way to better evaluate the interactions between phases and to link the micro-scale properties and phenomena to the quantities measured for the bulk material, as it needs much less simplifications than former analytical developments (such as [Frankel et al. 1967, Brule et al. 1991, Ancey et al. 1999]). This modeling can be based on lubrication models [Rognon et al. 2011], or more elaborated methods to reflect the fluid viscosity through pair interactions between particles [Yeo et al. 2010]. This is advantageous as it does not need to actually solve Navier-Stokes (NS) equations in the fluid phase. The price to pay is that long range interactions due to poromechanical couplings are difficult to reflect. An alternative is to really solve NS in the fluid phase using a CFD solver, or to use a lattice-Boltzman model [Ladd et al. 2001]. It is to be noted that direct resolution of NS does not eliminate the need for a proper modeling of the lubrication forces, due to mesh size dependencies [Nguyen et al. 2002]. The main difficulty associated to this approach is the high computational cost, so that following large deformations of thousands of immersed particles in 3D remains a challenging task.
A new method to simulate fluid-particle interactions has been developed recently and may be of some help to tackle the computational challenge [Catalano et al. 2013]. In this method, the solid phase is modelized with the discrete element method (DEM), and the fluid flow is solved using a pore-scale finite volume method (PFV). The key aspects of this DEM-PFV coupling are recalled in the first part of this paper. It was implemented in the open source code Yade-DEM [Smilauer et al. 2010]. Extensions of this method in order to study dense suspensions are being undertaken by the first author. Namely, the original model lacks a coupling term to link the fluid forces to the deviatoric strain, as explained hereafter. We also generalized the boundary conditions in order to allow very large deformations of the suspension in simple shear. Typical results of the preliminary enhanced model are presented in the last part.

NUMERICAL MODEL

Original DEM-PFV Coupled Model

Our DEM approach defines the mechanical properties of the interaction between grains whose shape is assumed to be spherical. Following Newton's laws, the positions of particles are updated and calculated at each time-step of the DEM simulation. As introduced in [Catalano et al. 2011], the PFV formulation is based on a simplified discretisation of the pore space as a network of regular triangulation and its dual Voronoi graph (figure 1).

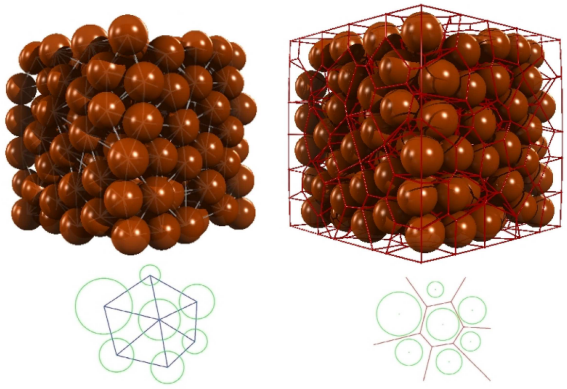

Figure 1: **Regular triangulation (left) and Voronoi graph (right).**

This network simplifies the formulation and resolution of the flow problem. The continuity equation is expressed for each pore, linking the rate of volume change of one tetrahedral element $\dot{V}_i^f$ to the fluxes q_{ij} through each facet. Each flux can be related to the pressure jump between to elements via a generalised Poiseuille's law, so that

$$\dot{V}_i^f = \sum_{j=j_1}^{j_4} q_{ij} = \sum_{j=j_1}^{j_4} K_{ij}(p_i - p_j) \tag{1}$$

couples the particles velocity to the fluid pressure field. The expression of conductivity K_{ij} has been validated recently by comparisons with glass beads experiments [Tong et al. 2012].
The total force exerted by the fluid on particle *k* can then be defined as [Chareyre et al. 2012]:

$$F^k = \int_{\partial\Gamma_k} p\, n\, ds + \int_{\partial\Gamma_k} \tau\, n\, ds \tag{2}$$

Lubrication forces

As classical poromechanics, the original DEM-PFV model takes into account the isotropic part of the stress and strain tensors (pressure and divergence of solid phase velocity) in the coupling (equation 1). The contribution of the fluid to the bulk shear stress is de facto neglected. It is worth noting that the shear part of the coupling is similarly lacking in discrete models inspired by the coupling equations of poromechanics, such as the continuum-discrete methods [Zeghal 2004, Zhao et al. 2013].
In order to deal with sheared suspensions, another viscous contribution has to be introduced for modeling the shear stress. Various ways may be used for this purpose such as viscous forces obtained in the framework of the lubrication theory. Lubrication effects are defined for all the elementary motions described in figure 2. Let's denote *k* and *k′* two particles in interaction of radius a_k and $a_{k'}$, linear velocities $\boldsymbol{v}_k$ and $\boldsymbol{v}_{k'}$ and angular velocities $\boldsymbol{\omega}_k$ and $\boldsymbol{\omega}_{k'}$, respectively. $a = (a_k + a_{k'})/2$ is their average radius and *h is* the inter-particle distance (surface to surface). The relative motions between the particles *k* and *k′* can be decomposed in four elementary motions corresponding to normal displacement (subscript *n*), shear displacement (*s*), rolling (*r*) and twisting (*t*). Lubrication forces and torques induced by these elementary motions are:

$$F_n^L = \frac{3}{2}\pi\eta\frac{a^2}{h}v_n \tag{3}$$

$$F_s^L = \frac{\pi\eta}{2}[-2a + (2a+h)\ln(\frac{2a+h}{h})]v_t \tag{4}$$

$$C_r^L = \pi\eta a^3(\frac{3}{2}\ln\frac{a}{h} + \frac{63}{500}\frac{h}{a}\ln\frac{a}{h})[(\omega_k - \omega_{k'})n] \tag{5}$$

$$C_t^L = \pi\eta a^2\frac{h}{a}\ln\frac{a}{h}[(\omega_k - \omega_{k'}).n]n \tag{6}$$

where $\mathbf{v}_n = ((\mathbf{v}_{k'} - \mathbf{v}_k)\cdot\mathbf{n})\mathbf{n}$ is the normal relative velocity, $\mathbf{v}_t = (a_k(\boldsymbol{\omega}_k - \boldsymbol{\omega}_n) + a_{k'}(\boldsymbol{\omega}_{k'} - \boldsymbol{\omega}_n))\times\mathbf{n}$ is an objective expression of the tangential relative velocity and $\boldsymbol{\omega}_n = (\boldsymbol{v}_{k'} - \boldsymbol{v}_k) \times \mathbf{n}/(a_k + a_{k'} + h)$ is the angular velocity of the local frame attached to the interacting pair. The normal and

shear forces, $\boldsymbol{F}_n$ and $\boldsymbol{F}_S$, are based on Frankel & Acrivos [Frankel et al. 1967, Brule et al. [1991] whereas C_r and C_t are based on Jeffrey & Onishi 1984. The reason of this choice will be discussed later. The total lubrication force $\boldsymbol{F}_k^L$ (resp. $\boldsymbol{F}_{k'}^L$) applied by particle k' on particle k (resp. by particle k on particle k') and the total torque $\boldsymbol{C}_k^L$ (resp. $\boldsymbol{C}_{k'}^L$) applied by particle k' on particle k (resp. by particle k on particle k') relative to the particle center read:

$$F_k^L = -F_{k'}^L = F_n + F_s \tag{7}$$

$$C_k^L = (a_k + \frac{h}{2}) F_s + C_r + C_t \tag{8}$$

$$C_{k'}^L = (a_{k'} + \frac{h}{2}) F_s - C_r - C_t \tag{9}$$

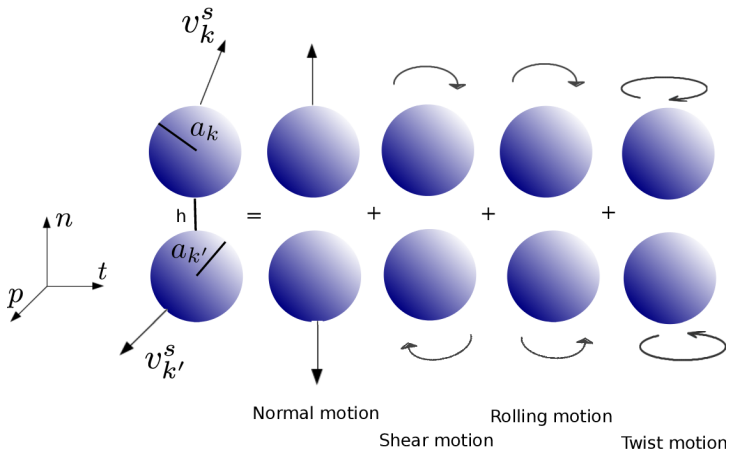

Figure 2: **Relative motion between particles [Marzougui et al. 2015].**

Figure 3 shows the comparaison of the FEM results performed on a simple configuration of identical spheres rotating at a given angular velocity, with that of equation 4 where F_S^L is determined alternatively using the expression from Jeffrey & Onishi ($F_s = \pi \eta a \ln \frac{a}{h}$) [8] and from Frankel & Acrivos 1967 (equation 4). Both expressions are asymptotically equivalent for $h \rightarrow 0$ but that of Frankel & Acrivos is in much better agreement with the FEM results for small h. The expression of Jeffrey & Onishi leads to negative torques for large h. This can alter the stability of the numerical scheme.

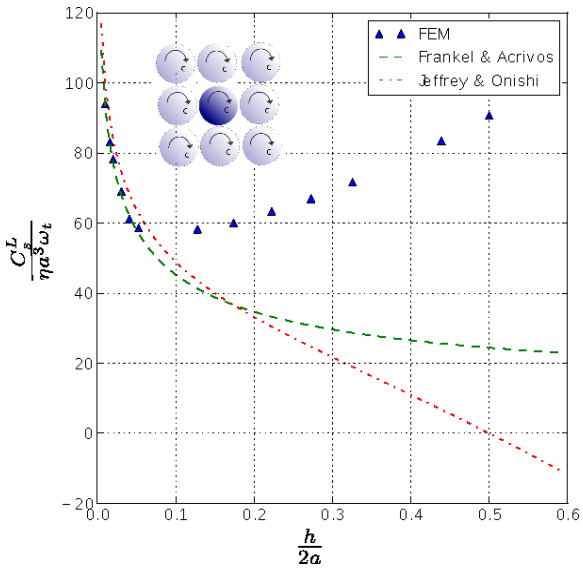

Figure 3: **Comparaison of viscous shear forces for the case of rotating sphere in a regular assembly of particles. h is the surface-to-surface distance and a is the particles radius [Marzougui et al. 2015].**

The normal interaction between two elastic-like particles in a viscous fluid is described by the Maxwell visco-elastic scheme (figure 4) which combines a spring of stiffness k in series with a pad of viscosity η. This combination between the lubrication and the elasticity is close to that adopted by Rognon [Rognon et al. 2011]. k_n is the contact stiffness and $v_n(h)$ is the instantaneous viscosity of the interaction as defined in eq. (3), such that $F_n^L = v_n(h)v_n$. The real velocity of approach between the two surfaces is $v_n - \dot{u}_n^e$, where $u_n^e = F_n^L / k_n$ is the elastic deformation. The evolution of the normal lubrication force obeys, then, the differential equation

$$\dot{F}_n^L = v_n(h)\left(v_n - \frac{\dot{F}_n^L}{k_n}\right) \tag{10}$$

Eq. 10 is integrated over time-steps using the form

$$\dot{F}_n^L = k_n\left(v_n - \frac{F_n^L}{v_n(h)}\right) \tag{11}$$

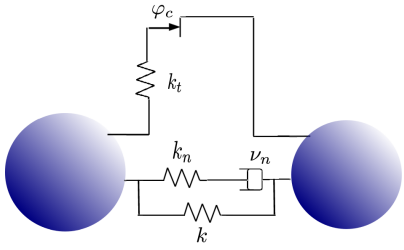

Figure 4: **Visco-elastic scheme of the interaction between two elastic-like particles [Marzougui et al. 2015].**

Periodic Boundary Conditions

As the system is considered infinite in the flow direction, some problems can arise from the boundary effects in the numerical simulation. In order to avoid such problems, periodic boundary conditions are implemented in the PFV model (figure 5) (the periodicity for the DEM part was developped independently). Denoting by $\mathbf{S} = [s_1,s_2,s_3]$ (figure 5) the period size in the three dimensions and by $\mathbf{i} \in \mathbb{N}^3$ is the distance between one point of coordinates $\mathbf{r}$ and its periodic image $\mathbf{r'} = \mathbf{r} + \mathbf{S} \cdot \mathbf{i}$ in an adjacent period, then the pore pressure is expressed as follow:

$$p' = p + \nabla p \,.S * i \tag{12}$$

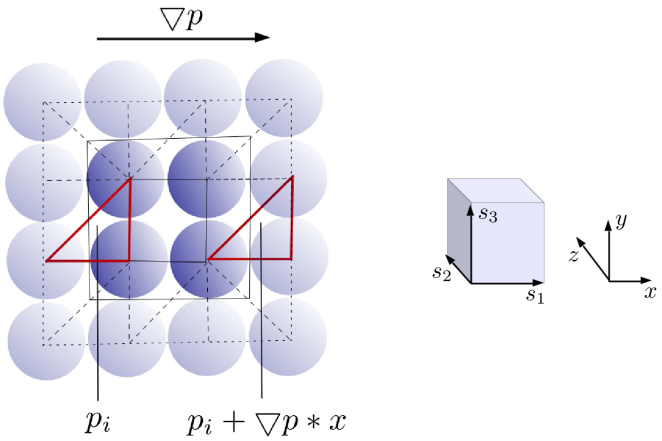

Figure 5: **(a): 2D periodic cell, (b): simulation period of size S = [s_1,s_2,s_3] in [x,y,z]**

NUMERICAL RESULTS

We generate an assembly of N=1000 frictional grains of average radius a = 0.025 ± 0.01 m, density $\rho = 2500 kg/m^3$ and friction angle $\Phi = 30°$. The assembly (Figure 6) is $H = 18a$ high, $L = 12a$ large and $l = 12a$ wide. The granular material is first confined under a constant vertical stress T_y, then sheared without gravity, between two parallel walls distant from H and moving at a velocity $\pm V/2 = 0.75 m/s$ respectively. In order to avoid slip zones near the plates, the first layer of spheres in contact with the plates is fixed to that ones by highly cohesive contacts. The boundary conditions for the top plate are the velocities $v_x = V/2$, $v_z = 0$, the total vertical stress T_y = 750 Pa and the fluid pressure $p = 0$. At the bottom plate, $v_x = -V/2$, $v_z = 0$ and the fluid velocity along the y axis $v_y^f = 0$. Periodic boundary conditions are applied along the horizontal axis for both the particles and the fluid. For the latest we impose a null pressure gradient at the macro-scale, i.e. $\nabla p_x = \nabla p_z = 0$.

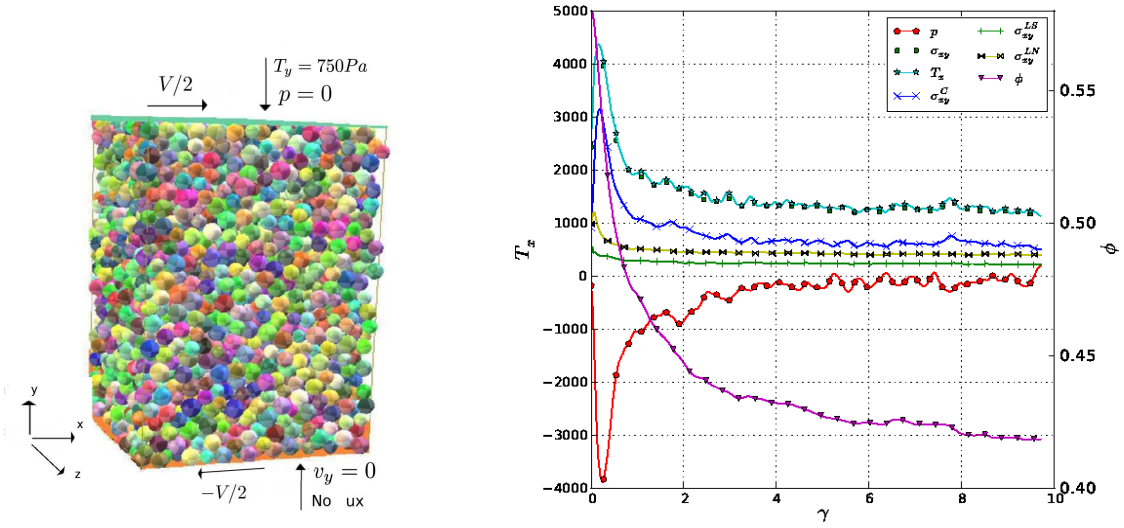

Figure 6: S**imulation cell (left). Evolution of the shear stress and the solid fraction as the deformation (right) [Marzougui et al. 2015].**

Simulations of such an assembly saturated of an incompressible fluid of viscosity η and submitted to a simple shear with shear rate $\dot{\gamma} = \frac{dV}{dH}$ at imposed vertical stress T_y are presented. The viscous stress is decomposed in different contributions which can be examined separately:

$$\sigma = \sigma^C + \sigma^L + p\,I + \sigma^I \tag{13}$$

$\sigma^C = \frac{1}{V}\sum F_{ij}^C \otimes l_{ij}$ is the contact stress applied on particles in contact where l_{ij} is the branch vector between particles *i* and *j*. $\sigma^L = \frac{1}{V}\sum F_{ij}^L \otimes l_{ij}$ is the lubrication stress [Ancey et al. 1999], which is the sum of the normal and shear components of the lubrication force. p is the pressure associated to the poromechanical coupling [Catalano et al. 2014]. $\sigma^I = \sum m_k v_k \otimes v_k$ reflect the inertial effects as defined in [Savage et al. 1981] where m_k and v_k are the mass and the velocity of particle k respectively. In figure 7, both $T_x = F_x / S$ (F_x is the force applied in the top plate and S is its area) and σ_{xy} are plotted and these two expressions compare consistently.

Figure 7 shows the different contributions of each force applied on the granular media for $I_v = 0.21$. The inertial stress σ_{xy}^I (not represented here) is negligible compared with the total stress ($\sigma_{xy}^I \ll 2.5\,T_x$). This indicates that the suspension is dominated by contacts and viscous interactions for the value of I_v investigated. The contact stress contributes to approximately half of the total stress. Contrary to what is sometimes postulated in the literature, our numerical results show that tangential lubrication forces ($\sigma_{xy}^{LT} \ll 20\,\%\,T_x$) are significant compared with the normal ones ($\sigma_{xy}^{LN} \ll 20\,\%\,T_x$).

The different contributions are investigated for different values of the viscous number I_v . I_v is a dimensionless form of the shear rate [Boyer et al. 2011], reflecting the magnitude of viscous effects, and is defined as:

$$I_v = \frac{\eta|\dot{\gamma}|}{T_y} \qquad (14)$$

The results obtained with only normal lubrication forces match qualitatively the empirical evolution of shear stress with I_v. However, the solid fraction obtained with this model is almost constant for $I_v \geq 0.02$, while the experiments suggest a monotonic decrease. The normal lubrication alone leads to a satisfactory stress ratio but overestimate the solid fraction. When the shear lubrication forces are included, the results get closer to the phenomenological laws $\mu(I_v)$ and $\phi(I_v)$. Consequently, the shear lubrication forces play a significant role to the dilatancy law, and they also contribute to the shear stress. The rolling torques, the twist torques and the poromechanical coupling have only marginal effects.

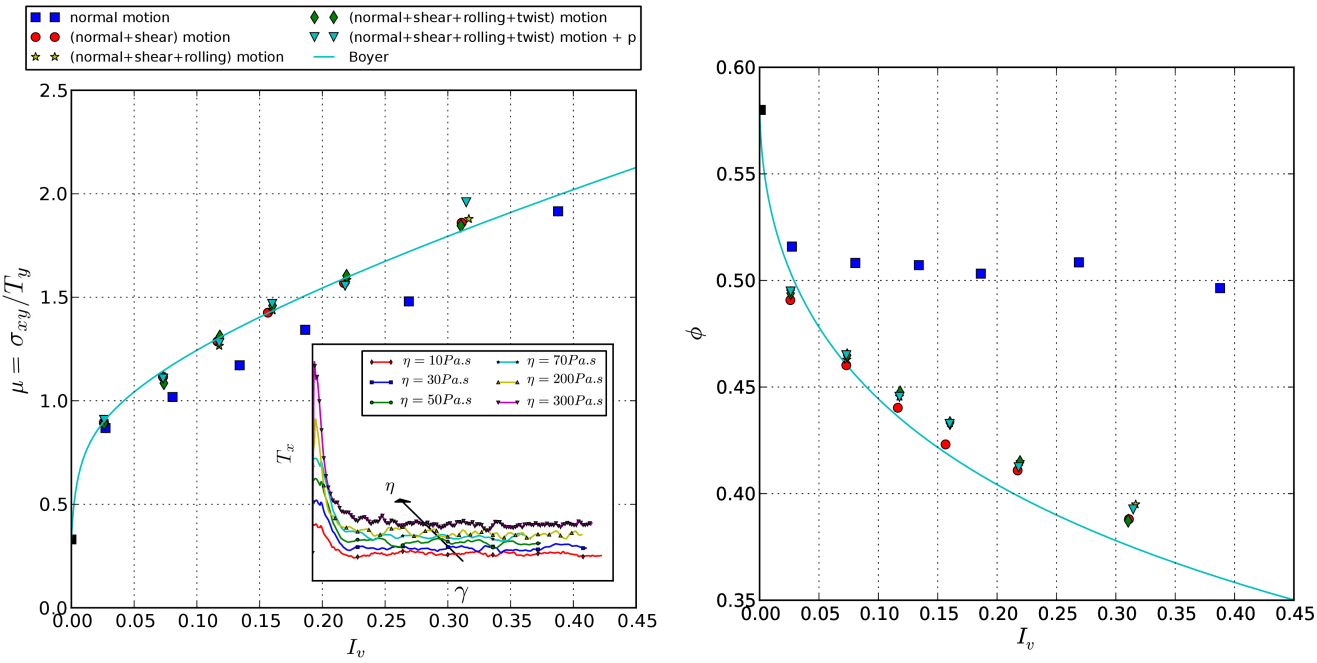

Figure 7: **Stress ratio μ (left) and the solid fraction φ (right) at steady state versus Iv . Each symbol represents a different combination of lubrication terms. The solid line is the phenomenological law of Boyer et al. 2011. Inset: the total shear stress for different values of fluid viscosity [Marzougui et al. 2015].**

CONCLUSION

In this contribution, we presented an original hydromechanical coupled model able to describe the behavior of dense granular materials subjected to a shear flow under constant pressure. The analysis of the various contributions to the bulk stress: contact forces, hydrodynamic forces and fluid pressure suggest that both the contact stress and the lubrication stress increase monotonically in the range of I_v investigated. The numerical model reproduces the behavior of dense suspensions described experimentally by the phenomenological laws from the experiments of Boyer et al [2] $\mu(I_v)$ and $\phi(I_v)$.

REFERENCES

Ancey, C., Coussot, P. and Evesque, P. (1978-present). A theoretical framework for granular suspensions in a steady simple shear flow. *Journal of Rheology* 43(6):1673–1699, 1999.

Boyer, F., Guazzelli, E. and Pouliquen, O. 2011. Unifying suspension and granular rheology. *Physical Review Letters*, 107(18):188301.

Catalano, E., Chareyre, B., Cortis, A., and Barthelemy, E. 2011. A Pore-Scale HydroMechanical Coupled Model For Geomaterials. In Onate, E. and Owen, D.R.J., editor, Particle-based methods II: Fundamentals and Applications, pages 798–809, 2011. *2nd International Conference on Particle-Based Methods - Fundamentals and Applications (Particles)*, Barcelona, Spain, oct 26-28.

Catalano, E., Chareyre, B. and Barthélémy, E. 2014. Pore- scale modeling of fluid-particles interaction and emerging poromechanical effects. *International Journal for Numerical and Analytical Methods in Geomechanics*, 38(1):51–71.

Chareyre, B., Cortis, A., Catalano, E. and Barthélémy, E. 2012 . Pore-scale modeling of viscous flow and induced forces in dense sphere packings. *Transport in Porous Media*, 92(2):473–493.

Frankel, N.A. and Acrivos, A. 1967. On the viscosity of a concentrated suspension of solid spheres. *Chemical Engineering Science*, 22(6):847–853.

Jeffrey, D.J. and Onishi, Y. 1984. Calculation of the resistance and mobility functions for two unequal rigid spheres in low-reynolds-number flow. *Journal of Fluid Mechanics*, 139:261–290.

Jeffrey, D.J. and Onishi, Y. 1984. The forces and couples acting on two nearly touching spheres in low-reynolds-number flow. *Zeitschrift fur angewandte Mathematik und Physik ZAMP*, 35(5):634–641.

Ladd, A.J.C. and Verberg, R. 2001. Lattice-boltzmann simulations of particle-fluid suspensions. *Journal of Statistical Physics*, 104(5-6):1191–1251.

Marzougui, D., Chareyre, B. and Chauchat, J., Microscopic origins of shear stress in dense fluid-grain mixtures, (to appear in) *Granular Matter*, (2015).

Nguyen, N-Q. and Ladd, A.J.C. 2002. Lubrication corrections for lattice-boltzmann simulations of particle suspensions. *Physical Review E*, 66(4):046708.

Rognon, P.G., Einav, I., Gay, C. 2011. Flowing resistance and dilatancy of dense suspensions: lubrication and repulsion. *Journal of Fluid Mechanics*, 689(1):75–96.

Savage, S.B. and Jeffrey, D.J. 1981. The stress tensor in a granular flow at high shear rates. *Journal of Fluid Mechanics*, 110:255–272.

Smilauer, V. and Chareyre, B. Yade Dem Formulation. In V. Smilauer, editor, *Yade Documentation*. The Yade Project, 1st edition, 2010. http://yade-dem.org/doc/.

Tong, A-T., Catalano, E., and Chareyre,B. 2012. Pore-Scale Flow Simulations: Model Predictions Compared with Experiments on Bi-Dispersed Granular Assemblies. *Oil & Gas Science and Technology-Revue d'IFP Energies Nouvelles*, 67(5):743–752.

Van den Brule, B. and Jongschaap, R.J.J. 1991. Modeling of concentrated suspensions. *Journal of statistical physics*, 62(5):1225–1237.

Yeo, K. and Maxey, M.R. 2010. Simulation of concentrated suspensions using the force-coupling method. *Journal of computational physics*, 229(6):2401–2421.

Zeghal, M. and El Shamy, U. 2004. A continuum-discrete hydromechanical analysis of granular deposit liquefaction. *International journal for numerical and analytical methods in geomechanics*, 28(14):1361–1383.

Zhao, J. and Shan T. 2013. Coupled CFD–DEM simulation of fluid–particle interaction in geomechanics. *Powder Technology*, 239(0):248 – 258.